SIAM J. NUMER. ANAL.
Vol. 50, No. 4, pp. 1899–1921

SHRINKING DIMER DYNAMICS AND ITS APPLICATIONS TO SADDLE POINT SEARCH*

JINGYAN ZHANG† AND QIANG DU†

Abstract. Saddle point search on an energy surface has broad applications in fields like materials science, physics, chemistry, and biology. In this paper, we present the shrinking dimer dynamics (SDD), a dynamic system which can be applied to locate a transition state on an energy surface corresponding to an index-1 saddle point where the Hessian has a negative eigenvalue. By searching for the saddle point and the associated unstable direction simultaneously in a single dynamic system defined in an extended space, we show that unstable index-1 saddle points of the energy become linearly stable steady equilibria of the SDD which makes the SDD a robust approach for the computation of saddle points. The time discretization of the SDD is connected to various iterative algorithms, including the popular dimer method used in many practical applications. Our study of these discretization schemes lays a rigorous mathematical foundation for the corresponding iterative saddle point search algorithms. Both linear local asymptotic stability analysis and optimal error reduction (convergence) rates are presented and further confirmed by numerical experiments. Global convergence and nonlinear asymptotic stability are also illustrated for some simpler systems. Applications of the SDD in both finite- and infinite-dimensional energy spaces are discussed.

Key words. saddle point search algorithms, shrinking dimer dynamics, dimer methods, linear stability, nonlinear stability, convergence analysis

AMS subject classifications. 37M05, 49K35, 37N30, 34K28, 65P99

DOI. 10.1137/110843149

1. Introduction.

Saddle point search has been of broad interest in many areas of scientific application, such as predicting nucleation rates in solid state transformation [19, 21, 29, 32] and computing transition rates in chemical reactions and computational biology [8, 14, 28].

There have been a variety of algorithms developed and successfully implemented to compute saddle points of a given energy surface. Generally speaking, methods for finding saddle points can be divided into chain-of-state methods involving two end states and surface walking methods from a single state [20]. Some typical examples of the former are given by the classical minimax method [27], the nudged elastic band method [17, 18], and the string method [10, 11], while examples of the latter include the gentlest ascent method developed in [7], the eigenvector-following method [6], the activation-relaxation technique [24], the trajectory-following algorithm [15, 30], the step and slide method [23], and the popular dimer method [16]. In comparison with the practical success of using these algorithms to probe complex energy surfaces in many large scale simulations, there has been relatively less mathematical development and rigorous numerical analysis, because much of the theory developed in the numerical analysis community has been devoted to problems with a prescribed saddle point structure (see [2] for a review and related references on the latter subject). This has begun to change as illustrated, for instance, by the studies of algorithmic convergence and stability in recent works [5, 12, 30].

*Received by the editors August 2, 2011; accepted for publication (in revised form) April 6, 2012; published electronically July 19, 2012. This research was partially supported by NSF grant DMS-1016073.

http://www.siam.org/journals/sinum/50-4/84314.html

†Department of Mathematics, Pennsylvania State University, University Park, PA 16802 (j_zhang@math.psu.edu, qdu@math.psu.edu).

In this paper, we mainly focus on formulating and analyzing continuous dynamics and discrete algorithms belonging to a special class of surface walking methods for locating saddle points, namely, that represented by the gentlest ascent method and the dimer method. The former was developed by Crippen and Scheraga [7] as an algorithm for moving from a minimum position on an energy surface to a neighboring minimum via an intervening saddle point. Recently, E and Zhou developed the gentlest ascent dynamics (GAD) as a dynamic system reformulation of the gentlest ascent method, and examined the linear stability of saddle points as the steady states [12]. While both the gentlest ascent method and GAD require the evaluation of second-order derivatives of the energy, the dimer method developed by Henkelman and Jonsson [16] uses only first-order derivatives of the energy, the so-called natural forces, via a dimer system consisting of two nearby points x_1 and x_2 separated by a small distance (that is, with a small dimer length $l = |x_2 - x_1|$). The dimer method works by alternately performing rotation and translation steps using only the gradient of the energy. Later it was argued that the method becomes more effective if the rotation step is performed until convergence for each translation step, instead of performing a single rotation after the translation [25]. The implementation was further improved by Kastner and Sherwood in [20] to achieve superlinear convergence for the rotation step by using the L-BFGS algorithm. They also reduced the number of gradient calculations per dimer iteration through an extrapolation of the gradients during repeated dimer rotations.

Motivated by the above works, we develop a shrinking dimer dynamics (SDD) to compute index-1 saddle points in this work. The original dimer method [16] may be viewed as a time discretization of the continuous SDD. This draws the analogy to the formulation of the GAD [12] as a continuous dynamic system corresponding to the (discrete) gentlest ascent method [7]. Indeed, adopting a dynamic system approach, such as a gradient flow of the energy, has been an immensely popular approach in both numerical optimization and mathematical analysis of variational problems. In the context of saddle point searching, the transformation to a continuous dynamic system has also been utilized in the literature to expedite the mathematical understanding; see, for instance, the analysis of string methods presented in [4] and the trajectory following method [15] for min-max saddle systems when the unstable modes can be identified a priori. For dimer methods, a dynamic system formulation was also proposed in [26] as second-order differential equations in time. Such transformations allow one to utilize many well-established tools from the dynamic system theory to rigorously analyze the convergence and stability properties of the underlying numerical algorithms. It is important to note that the unstable modes are generally unknown in practice; thus they must be computed as part of the solutions for some extended systems that provide the saddle position together with a characterization of its unstable (or stable) modes. The SDD gives a special example of such extended systems.

In the current work, we consider only index-1 saddle points which in the most generic setting correspond to transition states with the lowest energy barriers.[1] In addition, for an index-1 saddle point, only a single unstable direction of the corresponding Hessian needs to be identified, which leads to a smaller extended dynamic system, in comparison with the case of saddle points with higher indices. To make the converged steady state solution of the new dynamic system consistent with the saddle point, we introduce a dynamic reduction of the dimer length (thus a *shrinking dimer*) and gradually reduce the length to zero so that the probing of the unstable directions

[1] Here, an index-1 saddle refers to the critical point at which the Hessian of the energy functional has only one negative eigenvalue with the remaining eigenvalues all positive.

is done more locally (and accurately) as we get closer to the saddle point. This is an important point to make as a fixed dimer length has often been taken in many earlier studies, and we show that inappropriate choices may lead to the divergence of the SDD (and its time discretization). A full description of the SDD is given in section 2. Some mathematical studies of the SDD system are also conducted there with an emphasis on characterizing equilibrium states and investigating convergence and stability properties. The analysis of linear stability near an equilibrium is presented for the SDD in the same spirit as the analysis in [12] and [26]. These results are applicable to very general energy surfaces having reasonable regularity properties. Motivated by works like [15], we also illustrate that in some simplified cases, it is possible to obtain global convergence and nonlinear stability for the SDD. Such results, to our knowledge, are explored for the first time in the literature. When time discretization is considered in section 3, we make connections between the discrete SDD, in particular the various forms of the first-order Euler schemes, and the dimer method [16], and we provide theoretical analysis on both the convergence and the error reduction rates of the corresponding iterative algorithms. The theoretical analysis is complemented by a number of numerical experiments presented in section 4. The analytical results given here are new in the field. Moreover, they help us to gain a better understanding of a variety of popular saddle point search methods widely used in practice, such as the dimer method, and also motivate us to make further algorithmic advances. For instance, we present some variants of the numerical discretization to the SDD such as a semi-implicit time marching with a suitable splitting which can be potentially more effective for high-dimensional stiff problems. Finally, we conclude with some discussion on various possible generalizations in section 5.

2. Shrinking dimer dynamics. We begin with the formulation of the shrinking dimer dynamics (SDD). Then we present analytical discussions on linear and nonlinear stabilities associated with the SDD.

2.1. Formulation of the SDD. Consider a Hilbert space $\mathcal{H}$ which is compactly embedded in a Hilbert space $\mathcal{L}$, with $\mathcal{H}^*$ being the dual space of $\mathcal{H}$ with respect to the inner product (duality pairing) in $\mathcal{L}$. Let E be an energy functional defined in $\mathcal{H}$ and let $\nabla E(x)$ be the gradient of E at $x \in \mathcal{H}$ defined in the Fréchet sense with respect to the inner product in $\mathcal{L}$. Similarly, $H_E(x)$ is used to denote the Hessian operator of E at $x \in \mathcal{H}$.

Let x_1 and x_2 be two endpoints of a dimer (a line segment connecting the endpoints) in $\mathcal{H}$ with the dimer length $l = \|x_1 - x_2\|$. The dimer orientation is given by the unit vector $v = (x_1 - x_2)/l$, and the rotating dimer center is

$$x = (2-\alpha)x_1 + (\alpha - 1)x_2\,. \tag{2.1}$$

Here, the constant parameter $\alpha \in [1, 2]$ allows us to possibly pick the rotating center to be different from the geometric center, i.e., the midpoint of the dimer corresponding to $\alpha = 1.5$. Let

$$\begin{cases} F_1 = -\nabla E(x_1) = -\nabla E(x + (\alpha - 1)lv) \in \mathcal{H}^*, \\ F_2 = -\nabla E(x_2) = -\nabla E(x + (\alpha - 2)lv) \in \mathcal{H}^* \end{cases} \tag{2.2}$$

be the natural forces (negative gradients of the energy $E = E(x)$ with respect to x) evaluated at endpoints, and let

$$\begin{aligned} F_\alpha &= (2-\alpha)F_1 + (\alpha - 1)F_2 \\ &= (2-\alpha)F(x + (\alpha - 1)lv) + (\alpha - 1)F(x + (\alpha - 2)lv) \end{aligned} \tag{2.3}$$

be the approximated natural force at the rotating center of the dimer through a linear interpolation. The SDD system is given in the following form:

$$\begin{cases} \mu_1 \dot{x} = (I - 2vv^T)F_\alpha, \\ \mu_2 \dot{v} = (I - vv^T)(F_1 - F_2)/l, \\ \mu_3 \dot{l} = -\Gamma'(l), \end{cases} \tag{2.4}$$

where $\mu_1, \mu_2, \mu_3 > 0$ are positive relaxation constants. The notation vv^T, commonly used in linear algebra, is interpreted as $vv^T y = v^T y v$ for any $v \in \mathcal{H}$ and y in $\mathcal{H}^*$ with $v^T y = y^T v$ denoting symbolically the duality pairing (inner product) of v with y in $\mathcal{L}$. The term $\Gamma'(l)$, which is used to control the dimer length l, is the derivative of some artificial energy function $\Gamma = \Gamma(l)$ defined on $[0, +\infty)$.

The SDD system (2.4) is coupled with an initial condition:

$$x_\alpha(0) = x_0, \;\; v(0) = v_0, \;\; l(0) = l_0, \tag{2.5}$$

where $l_0 > 0$, $x_0 \in \mathcal{H}$, and v_0 is a unit vector in $\mathcal{H}$ with $\|v_0\| = 1$, with $\|\cdot\|$ denoting the norm of $\mathcal{L}$. More discussions on the choice of these parameters are given in section 4.

Geometrically and in comparison to the dimer method discussed in [16], the first equation in (2.4) represents the dimer translation step which can be viewed as a transformed gradient flow:

$$\mu_1 \dot{x} = \mathcal{Q}_v F_\alpha, \tag{2.6}$$

where $\mathcal{Q}_v = I - 2vv^T$ is the Householder transform that gives the mirror reflection with respect to the hyperplane perpendicular to the unit vector v. The geometric meaning is thus clear: while F_α moves the dimer center along the steepest descent direction, the result of mirror reflection, $\mathcal{Q}_v F_\alpha$ allows the dimer to climb up to the energy ascent direction characterized by the orientation vector. We thus see that geometrically one may replace $\mathcal{Q}_v$ by $I - \beta vv^T$ for any $\beta > 1$ while still achieving the same objective. If the unstable direction v is known a priori, then (2.6) is similar to the dynamic system studied in [15]. For most application problems, it is often the case that v is an unknown and interesting quantity which varies from different saddle points. Thus, the first equation needs to be complemented by an equation governing the vector v which is exactly the role played by the second equation.

Indeed, the second equation in (2.4) represents the dimer rotation step which tends to align the orientation vector v along the direction with the gentlest ascent. This is reflected in the term $(F_2 - F_1)/l$, which, for a small dimer length l, gives an approximated action of the Hessian at the dimer center along the direction v. Such a technique avoids the explicit calculation of the Hessian, which is one of the practical advantages of the dimer method [16] in comparison with other Hessian-based approaches. The idea is reminiscent of the use of a secant line as an approximation of the tangent while noticing that such an approximation is needed only along one particular direction. The projection operator

$$\mathcal{P}_v = I - vv^T \tag{2.7}$$

is used to ensure v is a unit vector at all time.

The third equation in (2.4) is a simple gradient flow system of the function Γ for the dimer length l. We require that $\Gamma = \Gamma(l)$ is monotonically increasing in l, with $l \equiv 0$ being the unique (and stable) equilibrium state. This simple gradient flow

controls how to shrink the dimer length while forcing it to approach zero. The latter is a necessary condition for the convergence of SDD to index-1 saddle points and the accurate local probing of the unstable direction. It is illustrated later in section 4.1 that, without meeting this condition, SDD may fail to converge. Generally, $\Gamma = \Gamma(l)$ is taken to increase at least superlinearly in l, but the form can be flexible. For example, two possible choices leading to different rates of decay in the dimer length are $\Gamma(l) = l^2/2$ corresponding to an exponential decay and $\Gamma(l) = l^4/4$ for a polynomial decay.

For much of the paper, the discussions are related to the studies of the steady state behavior of the SDD and its different discretization. We note that when $\mathcal{H}$ is a finite-dimensional Euclidean space (where most of the numerical simulations of saddle point search often take place), we have $\mathcal{H} = \mathcal{L} = \mathbb{R}^d$, and the well-posedness of the SDD (2.4) can be readily obtained for smooth energy functions. It is of theoretical interest to consider $\mathcal{H}$ being an infinite-dimensional space including Sobolev or other function spaces. In the latter case, we assume appropriate boundedness and smoothness of the natural force (gradient) and the Hessian operator so that the SDD (2.4) is well-posed in $L^2(0, \mathcal{T}; \mathcal{H}) \cap H^1(0, \mathcal{T}; \mathcal{H}^*)$ for any $\mathcal{T} > 0$. A systematic study on the well-posedness and the global long-time asymptotic behavior is beyond the scope of this work; however, our discussion in the remaining part of this section establishes a number of important mathematical properties of SDD, in particular, with respect to the problem of saddle point search of the underlying energy. To avoid technical complications, we assume that the gradient and the Hessian are all globally Lipschitz continuous. Such conditions can naturally be weakened for specific applications under consideration.

2.2. Analysis of linearly stable equilibria. In this section, we analyze linearly stable equilibria of SDD and their connections with index-1 saddle points. Here, linear stability refers to the standard stability notion of a linearized dynamic system at an equilibrium. Our discussions are made for different choices of relaxation constants due to the fact that they control how the systems approach their equilibria. This helps to guide us in developing methods to improve the efficiency when numerically implementing SDD, as discussed in section 4.

We note that in (2.4), if μ_3 is set to be zero and the limit $l \to 0$ is taken, then the SDD and its discretizations are reduced to single-end methods such as the gentlest ascent method [7] and the GAD [12], which require evaluations of the second-order derivatives of the energy. To avoid technical complications to the linear stability analysis due to possible degeneracies, we assume that the Hessian of the energy E at the saddle point of interests, H_E, has no zero eigenvalues, and we also assume that the second derivative $H_\Gamma = \Gamma''(0)$ of $\Gamma = \Gamma(l)$ at $l = 0$ is strictly positive, which is achieved by, for example, $\Gamma(l) = l^2/2$.

We now first show that linearly stable steady states of SDD in (2.4) are exactly index-1 saddle points. The proof is similar to the analysis given in [12] for the GAD; we include it here for completeness.

THEOREM 2.1. *Let x_1, x_2, x, v, l, E, F_1, F_2, F_α, and Γ be defined as above. If the SDD is given by* (2.4) *with $\mu_1, \mu_2, \mu_3 > 0$, then (x^*, v^*, l^*) is a linearly stable steady state of* (2.4) *if and only if*

1. *x^* is an index-1 saddle point of the energy E;*
2. *v^* is a unit eigenvector of the Hessian at x^*, $H_E(x^*)$, that corresponds to the smallest and only negative eigenvalue, λ^*.*
3. *l^* is 0.*

Proof. First, we show the necessary part. If (x^*, v^*, l^*) is a steady state of (2.4), it is obvious that $l^* = 0$ by the definition of $\Gamma = \Gamma(l)$. Setting the time derivative to zero, and noticing that as $l \to 0$, by the continuity assumptions, we have

$$0 = (2-\alpha)F_1 + (\alpha - 1)F_2 = F_\alpha \to F(x^*)$$

from the first equation of (2.4), so x^* must be a critical point of E. Moreover,

$$\lim_{l\to 0}(F_2 - F_1)/l = H_E(x^*)v^*$$

in the dual space $\mathcal{H}^*$. So, with $\|v^*\| = 1$, the second equation of (2.4) reduces to $H_E(x^*)v^* = (v^{*T}H_E(x^*)v^*)v^* = \lambda^* v^*$, which implies that v^* must be an eigenvector of $H_E(x^*)$.

In order to have the steady state being also a linearly stable one, we consider the Jacobian matrix (operator) J of the SDD,

$$J = \begin{pmatrix} \frac{1}{\mu_1}\mathcal{Q}_v\nabla_x F_\alpha & -\frac{2}{\mu_1}(vF_\alpha^T + v^T F_\alpha I) & \frac{1}{\mu_1}\mathcal{Q}_v\partial_l F_\alpha \\ \frac{1}{\mu_1 l}\mathcal{P}_v\nabla_x(F_1 - F_2) & J_{22} & \frac{1}{\mu_1 l}\mathcal{P}_v\partial_l(F_1 - F_2) \\ 0 & 0 & -\frac{1}{\mu_3}H_\Gamma \end{pmatrix}, \tag{2.8}$$

where ∂_l is the derivative with respect to l, I denotes the identity operator, and the center diagonal block J_{22} satisfies

$$\mu_1 J_{22} = \mathcal{P}_v\nabla_x((\alpha-1)F_1 + (2-\alpha)F_2) - v(F_1 - F_2)^T/l - (v^T(F_1 - F_2)/l)I\,.$$

At the steady state $(x^*, v^*, l^* = 0)$, $\nabla_x F_\alpha$ is equal to $-H_E(x^*)$, and the Jacobian becomes

$$\begin{pmatrix} \frac{1}{\mu_1}[2\lambda^* v^* v^{*T} - H_E(x^*)] & 0 & 0 \\ \frac{1}{\mu_2}[-H_E(x^*)v^* + (v^{*T}H_E(x^*)v^*)v^*] & \frac{2}{\mu_2}[\lambda^* v^* v^{*T} - H_E(x^*) + \lambda^* I] & 0 \\ 0 & 0 & -\frac{1}{\mu_3}H_\Gamma \end{pmatrix}.$$

By the assumption, we have $H_\Gamma > 0$ at the steady state. Since the Jacobian is lower triangular, let us now consider the spectrum of the first and the second diagonal blocks.

First, it is straightforward to check that v^* remains to be an eigenvector of $J_{11}^* = 2\lambda^* v^* v^{*T} - H_E(x^*)$ with the eigenvalue λ^*. Any other eigenvector u of $H_E(x^*)$, which is associated with an eigenvalue λ and is perpendicular to v^*, is also an eigenvector of J_{11}^* with eigenvalue $-\lambda$. So the eigenvalues of J_{11}^* are λ^* and the additive inverse of any other eigenvalue λ of $H_E(x^*)$.

Similarly, v^* remains an eigenvector of $J_{22}^* = 2\lambda^* v^* v^{*T} - H_E(x^*) + \lambda^* I$ with an eigenvalue $2\lambda^*$. Any other eigenvector u of $H_E(x^*)$ which is associated with a different eigenvalue λ is also an eigenvector of J_{22}^* perpendicular to v^* with an eigenvalue $\lambda^* - \lambda$. So the eigenvalues of J_{22}^* are $2\lambda^*$ and the differences between λ^* and any of the other eigenvalues λ of $H_E(x^*)$. We thus see that a necessary and sufficient condition for the diagonal blocks to have negative eigenvalues is that λ^* be the smallest and the only negative eigenvalue of $H_E(x^*)$ and v^* be the corresponding eigenvector. ∎

Before we end the analysis on the linear stability, we note that the above discussion can be extended to degenerate cases where one of the relaxation constants

μ_1 or μ_2 is set to be zero, which leads to DAE systems. One may take advantage of the Jacobians in (2.8) of the SDD being block lower triangular at steady states to investigate the linear stability of the DAE systems via corresponding subsystems of standard differential equations. In particular, the index-1 saddle points remain to be the only linearly stable steady states if the relaxation constant μ_2 is set to zero in (2.4), but the same conclusion is no longer valid if μ_1 is set to zero. In the latter case, the linearly stable steady states of (2.4) might be any critical point of the energy which is not a local minimum. As for the former case, we note that it corresponds to performing an instantaneous optimization on the orientation vector, which has been advocated in some previous works [20, 25].

2.3. Global convergence and nonlinear asymptotic stability. While the linear stability results offer strong evidence for the convergence of the SDD to an index-1 saddle point, it would surely provide more confidence if global convergence or nonlinear asymptotic stability can be established. Indeed, given the SDD as a dynamic system, a natural question is whether any of the stability concepts developed for nonlinear systems would be applicable to the study of the asymptotic behavior of the SDD. Here, we consider a simple energy defined by

$$E(x) = -z_1^2/2 + \sum_{i\neq 1} z_i^2/2 \tag{2.9}$$

for $x = (z_1, z_2, \ldots, z_d) \in \mathbb{R}^d$. In this case, there is a unique saddle point at the origin, and the gradient force is a linear map of the spatial variable x with the Hessian being a constant diagonal matrix with entries $(-1, 1, \ldots, 1)$ on the diagonal. Moreover, the SDD and the GAD systems [12] are identical to each other. We show that in this case, they lead to a globally convergent system for almost all initial data. Note that although the gradient force is linear, the SDD (or GAD) remains nonlinearly coupled.

THEOREM 2.2. *If the energy is given in* (2.9)*, then for any initial condition* $x_0, v_0 \in \mathbb{R}^d$ *such that* v_0 *is not perpendicular to the vector* $(1, 0, \ldots, 0)$*, the solution of SDD given by* (2.4) *will converge to* (x^*, v^*, l^*) *as* $t \to \infty$*, where*

1. $x^* = (0, \ldots, 0)$*;*
2. $v^* = (1, 0, \ldots, 0)$ *or* $v^* = -(1, 0, \ldots, 0)$*;*
3. $l^* = 0$.

Proof. First, we consider the second equation in (2.4), which can be written as

$$\mu_2 \begin{pmatrix} \dot{v_1} \\ \dot{v_2} \\ \cdots \\ \dot{v_d} \end{pmatrix} = \begin{pmatrix} 2v_1(1-v_1)(1+v_1) \\ -2v_1^2 v_2 \\ \cdots \\ -2v_1^2 v_d \end{pmatrix}. \tag{2.10}$$

From the equation for v_1 in (2.10), we can see that if initially $v_1 \in [-1, 1]$ and $v_1 \neq 0$, then v_1 will asymptotically converge to ± 1 as $t \to \infty$. And for $2 \leq i \leq d$, v_i will asymptotically converge to 0. Thus, we have either $v^* = (1, 0, \ldots, 0)$ or $v^* = -(1, 0, \ldots, 0)$. Next, we show that x^* is the origin. For the special energy, the first equation in the SDD (2.4) can be written as

$$\mu_1 \dot{x} = -Q_v Q_\infty x = -x + (Q_\infty - Q_v) Q_\infty x, \tag{2.11}$$

where

$$Q_\infty = \begin{pmatrix} -1 & 0 \\ 0 & I_{d-1} \end{pmatrix} \tag{2.12}$$

and $Q_v = I - 2vv^T \to Q_\infty$ as $t \to \infty$, since $v \to v^* = (\pm 1, 0, \ldots, 0)^T$. Thus, there exists a $\mathcal{T} > 0$ such that for any $t > \mathcal{T}$, we have $\|Q_v - Q_\infty\| \le 1/2$. Taking the inner product of (2.11) with x, we get

$$\frac{\mu_1}{2}|\dot{x}|^2 = x^T\dot{x} = -|x|^2 + x^T(Q_\infty - Q_v)Q_\infty x \le -\frac{1}{2}|x(t)|^2$$

for $t > \mathcal{T}$. So,

$$\mu_1|x(t)|^2 \le e^{-(t-\mathcal{T})}|x(\mathcal{T})|^2 \to 0 \text{ as } t \to \infty.$$

This finally gives $x^* = (0, \ldots, 0)$. The conclusion that $l^* = 0$ is obvious as the last equation of (2.4) decouples from remaining equations. ∎

3. Time discretization of SDD and numerical implementation. When numerically implementing the SDD (2.4), it is important to choose a proper discretization and parameters to obtain convergence. Our discussion in this section will not only cover the local stability/convergence property of the SDD, but also the global stability, as well as the optimal error reduction rate. We start from the simplest Euler scheme and then move on to other possible numerical schemes to improve the efficiency and the robustness of SDD. Since a discrete implementation of SDD is often formulated in finite dimension, to avoid technical complications, we consider only the case that $\mathcal{H}$ is a finite-dimensional Euclidean space with dimension d in this section. Same as for the continuous case, we assume that the Hessian of the energy E at any index-1 saddle point of interest has one negative eigenvalue and $d-1$ positive eigenvalues, and we also assume that $\Gamma(l) = l^2/2$ for simplicity.

We first introduce some notation. Let (x^*, v^*, l^*) be a stable steady state of SDD in (2.4). By Theorem 2.1, x^* is an index-1 saddle point and v^* is a unit eigenvector that corresponds to the smallest and only negative eigenvalue $\lambda^* < 0$ of $H_E(x^*)$. Let $\lambda_1 \le \lambda_2 \le \cdots \le \lambda_{d-1}$ be all of the remaining positive eigenvalues of $H_E(x^*)$, and let $|\lambda|_M = \max\{|\lambda^*|, |\lambda_{d-1}|\}$ and $|\lambda|_m = \min\{|\lambda^*|, |\lambda_1|\}$ denote the largest and the smallest absolute values of all eigenvalues, respectively.

3.1. Explicit Euler scheme for SDD: A discrete dimer method. Let Δt be the size of the time step and let (x^0, v^0, l^0) be the initial condition for SDD (2.4). Let

$$F_1^n = F(x^n + (\alpha - 1)l^n v^n), \tag{3.1}$$

$$F_2^n = F(x^n - (2 - \alpha)l^n v^n), \tag{3.2}$$

$$F_\alpha^n = (2 - \alpha)F_1^n + (\alpha - 1)F_2^n \tag{3.3}$$

be natural forces evaluated at the nth step. Notice that if $\Gamma(l) = l^2$, the third equation in (2.4) can be either analytically solved or we can use a fully implicit time stepping. Both lead to exponentially shrinking dimer length in time. Then by adopting an explicit Euler scheme for other equations in (2.4), we get the following iterative algorithm:

$$\begin{cases} x^{n+1} = x^n + \dfrac{\Delta t}{\mu_1}\mathcal{Q}_{v^n}F_\alpha^n, \\ v^{n+1} = v^n + \dfrac{\Delta t}{\mu_2 l^n}\mathcal{P}_{v^n}(F_1^n - F_2^n), \\ l^{n+1} = l^n \Big/ \left(1 + \dfrac{\Delta t}{\mu_3}\right). \end{cases} \tag{3.4}$$

The above scheme is similar to the iterations of the original dimer method [16] where the first equation resembles the translation step while the second is for the orientation. Note that if $\mu_2 = 0$, then an implicit scheme can be substituted in the orientation step to align the orientation to its instantaneous dynamic equilibrium direction. For $\mu_2 \neq 0$, the orientation step only approximates such a direction.

We note that the explicit Euler scheme does not preserve the unit length of v^n exactly. A simple modification can be made to ensure $\|v^n\| = 1$ holds in the discrete scheme without much complication, and detailed discussions are given in the next subsection.

Denote $\tilde{\mu_i} = \Delta t/\mu_i$, where $i = 1, 2, 3$, and

$$W(x, v, l) = \begin{pmatrix} x + \tilde{\mu}_1 \mathcal{Q}_v F_\alpha \\ v + \tilde{\mu}_2 l^{-1} \mathcal{P}_v (F_1 - F_2) \\ l/(1 + \tilde{\mu_3}) \end{pmatrix}, \tag{3.5}$$

where F_1, F_2, and F_α are defined as (2.2) and (2.3). It is not hard to see that (x^*, v^*, l^*) is a contractive fixed point of (3.5) for some properly chosen $\tilde{\mu_i}$ if and only if (x^*, v^*, l^*) is a stable steady state of SDD given by (2.4). The conditions for $\tilde{\mu_i}$'s to be satisfied lead to the asymptotic local stability analysis near a linearly stable steady state of (2.4), which also implies the local convergence of the iterative process as $n \to \infty$.

3.1.1. Local linear stability and convergence. The following theorem gives the asymptotic linear stability condition of the Euler scheme given by (2.4) near a linearly stable steady state.

THEOREM 3.1. *The numerical scheme given in* (3.4) *gives a local contraction (thus is asymptotically linearly stable) at a linearly stable steady state of SDD* (2.4)*, denoted by* (x^*, v^*, l^*)*, if and only if*

$$\Delta t < \min \left\{ \frac{2\mu_1}{|\lambda|_M}, \frac{2\mu_2}{|\lambda|_M - \lambda^*} \right\}. \tag{3.6}$$

Proof. The numerical scheme given by (3.4) is asymptotically stable at $(x^*, v^*, 0)$ if and only if all eigenvalues of the Jacobian matrix of W at (x^*, v^*, l^*) stay inside the unit disc. Note that the Jacobian matrix of W at $(x^*, v^*, 0)$ reads like

$$J_W|_{(x^*, v^*, 0)} = \begin{pmatrix} I + \tilde{\mu}_1 J_{11} & 0 & 0 \\ * & I + \tilde{\mu}_2 J_{22} & 0 \\ 0 & 0 & (1 + \tilde{\mu_3})^{-1} \end{pmatrix}, \tag{3.7}$$

where a detailed expression for a subdiagonal block is ignored and the diagonal blocks are $J_{11} = 2\lambda^* v^* v^{*T} - H_E(x^*)$ and $J_{22} = 2\lambda^* v^* v^{*T} - H_E(x^*) + \lambda^* I$ as computed before. The eigenvalues of $J_W|_{(x^*, v^*, l^*)}$ are thus in the following form:

$$1 - \tilde{\mu}_1 |\lambda|, \quad 1 - \tilde{\mu}_2 (|\lambda| - \lambda^*), \quad (1 + \tilde{\mu_3})^{-1},$$

where λ is any one of the eigenvalues of $H_E(x^*)$. Thus, by setting all of the above values inside $(-1, 1)$, we get

$$\tilde{\mu}_1 < \frac{2}{|\lambda|_M} \text{ and } \tilde{\mu}_2 < \frac{2}{|\lambda|_M - \lambda^*},$$

which is exactly (3.6). ∎

From the above, we can estimate the upper bound of the size of the time step allowable to get a local contraction, and we can see that it depends on the extreme eigenvalues of the Hessian at x^*, as well as μ_1 and μ_2. A concrete example is provided in section 4.1 to verify the above estimation. Moreover, we can show that only index-1 saddle points and their unstable directions are the contractive fix points of the Euler scheme since at any other fixed point, the Jacobian always has an eigenvalue strictly larger than 1. We give a theorem below, and the proof is similar to the one given above.

THEOREM 3.2. *If x^* is any critical point of the energy functional E other than index-1 saddle points and v^* is an associated unit eigenvector of $H_E(x^*)$, then $(x^*, v^*, 0)$ is a fixed point of the Euler scheme, but not contractive.*

3.1.2. Optimal error reduction rate. Theorem 3.1 gives the largest step size allowable to get the local contraction or the linear asymptotic stability of the numerical scheme (3.4). The next question is to ask what the optimal time step size is, in the sense that an optimal error reduction rate can be achieved.

Let $(x^*, v^*, l^* = 0)$ be a steady state of (3.4) and let $z^n = (x^n, v^n, l^n)$ be the numerical solution at the nth step. Since we are mostly interested in the accuracy of the approximations to x^* and v^*, we define the error reduction rate as

$$r = \lim_{n\to\infty} \frac{\|(x^{n+1} - x^*, v^{n+1} - v^*)\|}{\|(x^n - x^*, v^n - v^*)\|}. \tag{3.8}$$

The following theorem gives an estimation of the optimal error reduction rate when (3.4) approaches its steady state. It provides some guidelines for choosing the relaxation constants, as well as the time step, to achieve the optimal rate.

THEOREM 3.3. *At a linearly stable steady state $z^* = (x^*, v^*, 0)$ of the SDD* (2.4)*, for the explicit Euler scheme* (3.4)*, the error reduction rate given by* (3.8) *satisfies*

$$r \geq r_{op} = \frac{|\lambda|_M - |\lambda|_m}{|\lambda|_M + |\lambda|_m}. \tag{3.9}$$

The optimal error reduction rate can be achieved when

$$\Delta t = \frac{2\mu_1}{|\lambda|_m + |\lambda|_M}, \tag{3.10}$$

$$\left(1 + \frac{|\lambda^*|}{|\lambda|_M}\right)\mu_1 < \mu_2 < \left(1 + \frac{|\lambda^*|}{|\lambda|_m}\right)\mu_1 . \tag{3.11}$$

Proof. By linearization, the error reduction rate is determined by $\tilde{J}_W(x^*, v^*)$, the projected Jacobian matrix with respect to x and v. By the computation given in the proof of Theorem 3.1, we have

$$r = \max\{|1 - |\lambda|\tilde{\mu}_1|, |1 - |\lambda|\tilde{\mu}_2|\},$$

where $\tilde{\mu}_1 = \Delta t/\mu_1$, $\tilde{\mu}_2 = \Delta t/\mu_2$, and λ is any eigenvalue of the Hessian $H_E(x^*)$. Thus, the optimal error reduction rate is

$$r_{op} = \min_{\{\tilde{\mu}_i\}} \max_{\lambda} \max\{|1 - |\lambda|\tilde{\mu}_1|, |1 - |\lambda|\tilde{\mu}_2|\}. \tag{3.12}$$

On one hand, we have $\max\{|1 - |\lambda|\tilde{\mu}_1|, |1 - |\lambda|\tilde{\mu}_2|\} \geq |1 - |\lambda|\tilde{\mu}_1|$, thus

$$r_{op} \geq \min_{\tilde{\mu}_1} \max_{\lambda} \{|1 - \tilde{\mu}_1|\lambda||\}. \tag{3.13}$$

It is not hard to see that the minimum of the right-hand side of (3.13) is achieved when $1-\tilde{\mu}_1|\lambda|_M = -(1-\tilde{\mu}_1|\lambda|_m)$; thus, we can see

$$r_{op} \geq \min_{\tilde{\mu}_1} \max_{\lambda} \{|1-\tilde{\mu}_1|\lambda||\} = \frac{|\lambda|_M - |\lambda|_m}{|\lambda|_M + |\lambda|_m},$$

where the equality holds when $\tilde{\mu}_1 = \Delta t/\mu_1$ satisfies (3.10).

On the other hand, we may check that if $\tilde{\mu}_2 = \Delta t/\mu_2$ satisfies (3.11), then $|1-\tilde{\mu}_2|\lambda|| \leq (|\lambda|_M - |\lambda|_m)/(|\lambda|_M + |\lambda|_m)$ for any λ. Thus, when (3.10)–(3.11) are satisfied, an error reduction rate of $(|\lambda|_M - |\lambda|_m)/(|\lambda|_M + |\lambda|_m)$ can be obtained. ∎

Numerical verification of the above estimation is given in section 4.1.

3.2. Modified Euler scheme for SDD. Note that the second equation in the SDD contains a Lagrangian multiplier for the constraint that $\|v(t)\|_2 = 1$. This motivates us to consider a modified Euler Scheme which performs a normalization on v at each step. To be more specific, the modified scheme is given in the following:

$$\begin{cases} x^{n+1} = x^n + \tilde{\mu}_1 \mathcal{Q}_{v^n} F_\alpha^n, \\ \tilde{v}^{n+1} = v^n + \tilde{\mu}_2 (F_1^n - F_2^n)/l^n \,, \\ v^{n+1} = \tilde{v}^{n+1}/\|\tilde{v}^{n+1}\| \,, \\ l^{n+1} = l^n/(1+\tilde{\mu}_3), \end{cases} \tag{3.14}$$

where $\tilde{\mu}_i = \Delta t/\mu_i$ for $i = 1, 2, 3$ and F_1^n, F_2^n, and F_α^n are the same as those defined in (3.1)–(3.3). Due to the normalization step, this modified scheme can explicitly guarantee the condition that $\|v^n\| = 1$, while maintaining or improving the local stability and optimal error reduction rate as demonstrated next.

3.2.1. Local linear stability and convergence. The following theorem shows that the modified Euler scheme is locally linearly asymptotically stable if the time step Δt satisfies a certain stability condition that is weaker than the one needed for the Euler scheme discussed previously.

THEOREM 3.4. *The numerical scheme given by* (3.14) *gives a local contraction (thus is asymptotically linearly stable) at a linearly stable steady state of SDD* (2.4)*, denoted by* $(x^*, v^*, 0)$*, if and only if*

$$\Delta t < \min\left(\frac{2\mu_1}{|\lambda|_M}, \frac{2\mu_2}{\lambda_{d-1}}\right) . \tag{3.15}$$

Proof. Similar as before, we consider the Jacobian matrix, denoted by J_M, of the map determined by the modified Euler scheme (3.14) at $(x^*, v^*, 0)$. We can write J_M at the steady state $(x^*, v^*, 0)$ in the following form:

$$J_M = \begin{pmatrix} J_{11} & 0 & 0 \\ * & J_{22} & 0 \\ 0 & 0 & J_{33} \end{pmatrix},$$

where J_{11} is the same as in the proof of Theorem 3.1 and J_{33} is a negative number. So, here we only calculate J_{22}. Let $F(v^n) := v^n + \tilde{\mu}_2(F_1^n - F_2^n)/l^n$ and $K(\tilde{v}^n) := \tilde{v}^n/\|\tilde{v}^n\|_2$. We then have $v^{n+1} = (K \circ F)(v^n)$, and J_{22} is the Jacobian of $(K \circ F)$ at the steady state which can be computed by

$$J_{22} = \left(-\frac{v^* v^{*T}}{(v^{*T} v^*)^{3/2}} + \frac{1}{(v^{*T} v^*)} I\right)(I - \tilde{\mu}_2 H_E(x^*)) \,. \tag{3.16}$$

Thus, by similar calculation as in the proof of Theorem 3.1, we can show that the eigenvalues of J_{22} are 0 and $\{1-\tilde{\mu}_2\lambda_i\}$, and thus the eigenvalues of J_M at $(x^*, v^*, 0)$ are

$$1+\tilde{\mu}_1\lambda^*, 1-\tilde{\mu}_1\lambda_i, 0, 1-\tilde{\mu}_2\lambda_i\,,$$

where λ^* and λ_i $(i=1,\ldots,d-1)$ are eigenvalues of $H_E(x^*)$ as defined before. To make all of them stay in $(-1,1)$, we need

$$\tilde{\mu}_1 < \frac{2}{|\lambda|_M} \quad \text{and} \quad \tilde{\mu}_2 < \frac{2}{\lambda_{d-1}},$$

which is exactly (3.4). ∎

Moreover, we show later that the optimal error reduction rates of both the Euler and the modified Euler schemes are the same, and the only difference is that the ranges for the choices of μ_2 to achieve the optimal error reduction rate are different.

3.2.2. Optimal error reduction rate. Similar to the Euler scheme, the following theorem holds for the modified Euler scheme.

THEOREM 3.5. *At a linearly stable steady state $z^* = (x^*, v^*, 0)$ of SDD* (2.4)*, for the modified Euler scheme* (3.14)*, the error reduction rate given by* (3.8) *satisfies*

$$r \geq r_{op} = \frac{|\lambda|_M - |\lambda|_m}{|\lambda|_M + |\lambda|_m}. \tag{3.17}$$

The optimal error reduction rate can be achieved when

$$\Delta t = \frac{2\mu_1}{|\lambda|_m + |\lambda|_M}\,, \tag{3.18}$$

$$\frac{\lambda_{d-1}}{|\lambda|_M}\mu_1 \leq \mu_2 \leq \frac{\lambda_1}{|\lambda|_m}\mu_1\,. \tag{3.19}$$

Proof. The proof is similar to that for Theorem 3.3. ∎

We note that both [20] and [25] suggested that it is advantageous to keep rotating the dimer until convergence, rather than to perform a single rotation and a single translation alternately. For the SDD, as indicated earlier in the linear stability analysis of the dynamic system, this corresponds to the case $\mu_2 = 0$. Our above analysis shows that the optimal error reduction rate, as measured by the errors of both the shrinking dimer (saddle point) position and the dimer orientation, is dominated by the consideration for the dimer position when the SDD is approaching its steady state. Moreover, a good choice of the relaxation constant for the rotation steps of SDD can be as effective as carrying out a complete optimization process. For the modified Euler scheme, we note that a particular choice of $\mu_2 = \mu_1$ is always in the feasible range of (3.19). Naturally, the conclusion reached here is for iterative algorithms based on the simple Euler-type schemes for the dimer position, which is at best linearly convergent. A possible acceleration is possible if methods with superlinear convergence can be implemented in ways that can improve the efficiency while maintaining robust convergence properties like the ones demonstrated here.

3.2.3. Global convergence and nonlinear stability. Similar to the discussion of global convergence and the asymptotic nonlinear stability in section 2.3 for the continuous SDD, we can also study the stability and the contractive feature of discrete schemes. Again, we consider the simple energy defined by (2.9).

THEOREM 3.6. *Given the energy as in* (2.9)*, the modified Euler scheme converges to the globally stable steady state given by* (2.2) *if* v_0 *is chosen not to be perpendicular to* $(1, 0, \ldots, 0)$ *and* $\Delta t < 2\mu_1$.

Proof. First, we get by (3.23) that

$$\tilde{v}^{n+1} = \begin{pmatrix} 1+\tilde{\mu}_2 & 0 \\ 0 & (1-\tilde{\mu}_2)I_{d-1} \end{pmatrix} v^n. \tag{3.20}$$

After normalization, it is not hard to see that $v^n \to (\pm 1, 0, \ldots, 0)^T$ as $n \to \infty$ if v_0 is not perpendicular to $(1, 0, \ldots, 0)$. This is reminiscent of the convergence of the power method for solving the algebraic eigenvalue problem.

Next, by the first equation in the modified scheme (3.23), we have

$$x^{n+1} = x^n - \tilde{\mu}_1 \mathcal{Q}_{v^n} Q_\infty x^n = -\tilde{\mu}_1 (\mathcal{Q}_{v^n} - Q_\infty) Q_\infty x^n + (1-\tilde{\mu}_1) x^n,$$

where Q_∞ is defined as in (2.12). Since $\mathcal{Q}_{v^n} = I - 2v^n v^{nT} \to Q_\infty$ as $n \to \infty$, we get

$$\|x^{n+1}\| \le \tilde{\mu}_1 \|(\mathcal{Q}_{v^n} - Q_\infty) Q_\infty x^n\| + |1-\tilde{\mu}_1| \|x^n\|. \tag{3.21}$$

For $\tilde{\mu}_1 = \Delta t/\mu_1 < 2$, there exists a small positive number $\epsilon < \min(2-\tilde{\mu}_1, \tilde{\mu}_1)$ such that $|1-\tilde{\mu}_1| \le 1-\epsilon$. Meanwhile, for $\epsilon > 0$, there exists an $N > 0$ such that if $n > N$,

$$\tilde{\mu}_1 \|(\mathcal{Q}_{v^n} - Q_\infty) Q_\infty x^n\| \le \frac{\epsilon}{2} \|x_n\|.$$

Thus, (3.21) becomes

$$\|x^{n+1}\| \le \left(1 - \frac{\epsilon}{2}\right) \|x^n\|,$$

which implies that $\|x^n\| \to 0$ as $n \to \infty$ if $\Delta t < 2\mu_1$. ∎

3.3. Semi-implicit splitting scheme for the SDD. Explicit Euler-type methods are quite easy to implement. However, the time step has to be small enough to satisfy the stability condition. This highly affects the efficiency of the SDD, especially when high-dimensional energy landscapes are considered. Thus, a semi-implicit splitting scheme is presented in this section to improve the convergence of SDD to desired saddle points in the numerical implementation.

For $x \in \mathcal{H}$, let $F(x) = -\nabla E(x)$ be written as

$$F(x) = F_L(x) + F_N(x), \tag{3.22}$$

where F_L denotes a linear map of x while F_N includes the rest of the terms that may possibly be nonlinear. Letting $F_{iN} = F_N(x_i)$ for $i = 1, 2$, we get

$$\begin{aligned} &(2-\alpha)F_1 + (\alpha-1)F_2 = F_L(x) + (2-\alpha)F_{1N} + (\alpha-1)F_{2N} =: F_L(x) + F_{\alpha N}, \\ &l^{-1}(F_1 - F_2) = F_L(v) + l^{-1}(F_{1N} - F_{2N}). \end{aligned}$$

A semi-implicit scheme is then given by

$$\begin{cases} x^{n+1} = x^n + \tilde{\mu}_1 \mathcal{Q}_{v^n}(F_L(x^{n+1}) + F^n_{\alpha N}), \\ \tilde{v}^{n+1} = v^n + \tilde{\mu}_2 (F_L(\tilde{v}^{n+1}) + (F^n_{1N} - F^n_{2N})/l^n), \\ v^{n+1} = \tilde{v}^{n+1}/\|\tilde{v}^{n+1}\|, \\ l^{n+1} = l^n/(1+\tilde{\mu}_3)\ . \end{cases} \tag{3.23}$$

Note that, in general, there are many semi-implicit schemes depending on the use of different splitting strategies. We may take a very general view of the splitting (3.22) that allows one to treat F_L implicitly and F_N explicitly. Sometimes a fully implicit scheme can also be used where the orientation step is very much similar to the normalized gradient flow scheme analyzed in [1]. Here, our main goals are to reduce the stiffness of the SDD system, thus allowing a larger time step size, and to obtain better error reduction, thus being more effective in convergence to the steady state. A detailed analysis of the various splitting strategies and their effectiveness will be pursued in our future works; however, a concrete example is provided in section 4.3 as an illustration for a possible choice of a semi-implicit scheme.

4. Numerical experiments and applications. In this section, we give some numerical examples to show how the SDD is implemented numerically. Let us first address the choices of the parameters used in the SDD besides those already discussed in the analysis given earlier.

First, about the rotating center given by (2.1) with $1 \leq \alpha \leq 2$, when $\alpha = 1$ or 2, the rotating center is one of the endpoints of the dimer, and this corresponds to the algorithm given by [20], where only forces at the center and one endpoint of the dimer are evaluated, which may potentially reduce the number of gradient evaluations per iteration, yet the order of approximation to the action of the Hessian along the dimer orientation direction becomes one order lower than when using the midpoint as the rotating center, i.e., $\alpha = 1.5$. The flexibility of the choice of the dimer center becomes more important when we consider the generalized dimer dynamics for locating saddle points of higher-order indices, with the main difference being the use of k-dimensional hypercubes or k-dimensional simplices for a saddle point of index k.

Concerning the initial position of the dimer, it is obviously better to choose x_0 to be close to x^* if some a priori information is available, and v_0 can be obtained by performing the rotation step until convergence to an eigenvector associated with the lowest eigenvalue of the Hessian at x_0, which is equivalent to solving the second equation in (2.4) by fixing $x = x_0$. However, when no a priori information on x^* is known and x_0 is potentially far from a saddle, then there is no advantage to aligning v_0 in the direction corresponding to the eigenvector of the lowest eigenvalue of the initial Hessian, since the Hessian at x_0 might be quite different from that at x^*. As for the initial dimer length, it obviously depends on the particular energy surface. We mostly assign it a relatively small value and, as the iteration goes, the dimer length shrinks automatically. Since a difference quotient of the natural forces is used in the SDD, whenever possible, care is taken to avoid the loss of significant digits in the arithmetic operations. We note that in the examples we have considered, the numerical convergences are reached, that is, the dynamic iterations of the dimer are terminated, without any numerical instability being observed.

4.1. A two-dimensional example. In the SDD, the dimer length approaches zero at the steady state. We have theoretically shown in section 2 that this condition is necessary for the convergence of the SDD to index-1 saddle points. The dependence on the time step size of the convergence and the optimal error reduction rates for various discrete schemes associated with the SDD have also been discussed in section 3. As an illustration, we consider the two-dimensional energy landscape given by $E(x, y) = (x^2 - 1)^2 + y^2$, so that $(\pm 1, 0)$ are the two local minima and $(0, 0)$ is the

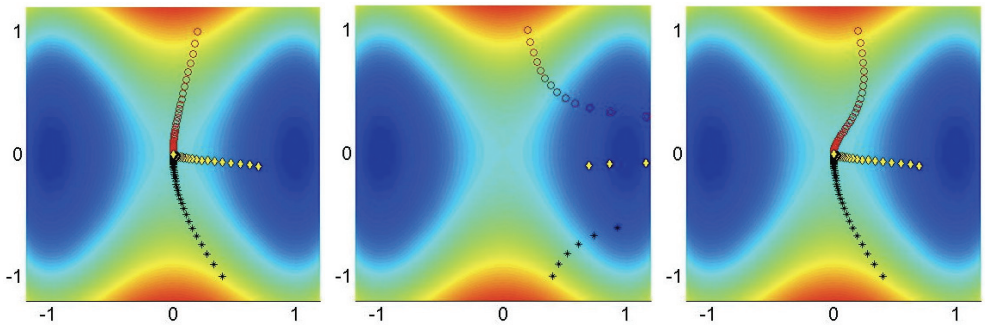

FIG. 4.1. *Left: with a fixed $l = 0.4$ (convergent). Middle: with a fixed $l = 0.7$ (divergent). Right: shrinking dimer with initial length $l_0 = 0.7$ (convergent).*

index-1 saddle point. The Hessian matrix of $E(x, y)$ is

$$H_E(x, y) = \begin{pmatrix} 12x^2 - 4 & 0 \\ 0 & 2 \end{pmatrix}. \tag{4.1}$$

The dimer orientation v at the steady state of (2.4) is a unit eigenvector of $H_E(0, 0)$ that corresponds to the smallest and the only negative eigenvalue -4, i.e., $v^* = (\pm 1, 0)$. So, the steady state of (2.4) is $(x^*, v^*) = (0, 0, \pm 1, 0)$. The following test runs illustrate the effect of the dimer length on the trajectory of the dimer system for the simple energy landscape considered here. In all three pictures shown in Figure 4.1, we take the same set of initial positions and directions: $(x_0, v_0) = (0.2, 1, 1, 0)$, $(0.4, -1, 1, 0)$, and $(0.7, -0.1, 1, 0)$. The left one takes a small fixed dimer length of $l = 0.4$, while in the middle one a larger but also fixed dimer length $l = 0.7$ is used. We can see that if the dimer length is fixed to be a relatively large number, it might not converge to the saddle point. In the right picture, we allow the shrinkage of the dimer length with an initial length $l_0 = 0.7$ being used so the convergence is always achieved.

To better understand the above observations, we revisit the linear stability analysis of the SDD for this special two-dimensional energy landscape. The fixed length dimer system, which is equivalent to the system consisting of the first two equations of (2.4), shows that although $(0, 0, \pm 1, 0)$ is still a fixed point, the stability at this point depends on l. To be more specific, the Jacobi matrix of the right-hand side map of the SDD is actually a diagonal matrix with diagonal entries $(12l^2-4, -2, 2(4l^2-4), 4l^2-6)$, respectively. Thus, we can see that only if $l^2 < 1/3$ can this system be assured to converge to the index-1 saddle point $(0, 0)$. This agrees with the numerical observations.

The example suggests that when a fixed length dimer system is implemented, the dimer length needs to be carefully chosen. Often in practical problems, especially for high-dimensional energy landscape, it is not straightforward to determine a priori a dimer length small enough for the convergence. However, the SDD can resolve this issue because the dimer length is systematically reduced and is forced to be zero asymptotically, which guarantees the theoretical convergence of the SDD. Of course, as discussed earlier, we advocate the users to exercise best practice in the numerical evaluation of the force difference at the endpoints; for instance, if exceedingly small dimer length must be used for the SDD, alternative forms of the difference quotient (perhaps through a more direct evaluation of the Hessian action, or a suitable part of the Hessian action) may be considered to reduce any possible effect of rounding error at the cost of more expensive computation.

Next, we verify the theoretical results on the largest time step size allowable to maintain the local stability and the optimal time step size for the most significant error reduction rate given earlier. We take the explicit Euler method with the initial guess chosen to be close to the steady state. In particular, we let $x_0 = (0.9, 0.1)$, $v_0 = (9,1)/\sqrt{82}$, and $l_0 = 10^{-5}$. Based on the analysis given by (3.6), the largest possible time step size is $\Delta t = 0.25$ and the optimal time step size is $\Delta t = 0.2$, with the optimal error reduction rate 0.6. Here, the error reduction rate at the nth step is calculated by $r_n = \|e^{n+1}\|/\|e^n\|$, where $\|e^n\|^2 = \|x^n - x^*\|^2 + \|v^n - v^*\|^2$. This does not account for the change in the dimer length which carries no physical significance. The error reduction rates corresponding to different sizes of the time step Δt (referred to as dt) are given in Figures 4.2 and 4.3.

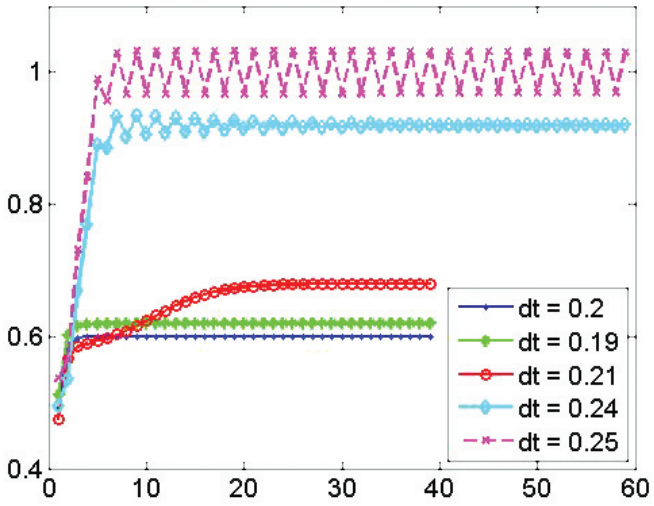

FIG. 4.2. *Error reduction rates for different time step sizes with the Euler scheme.*

For the pictures in Figure 4.2 and 4.3, the relaxation constants are taken as $\mu_1 = \mu_2 = \mu_3 = 1$. We note from Figure 4.2 that if the Euler scheme is applied, when $\Delta t = 0.2$, the error reduction rate can get 0.6, which is the smallest one among the different Δt's; also, when Δt is increased to 0.25, the error reduction rate is nearly 1, and thus the explicit Euler scheme fails to reach the steady state. However, in Figure 4.3 where the modified Euler scheme is applied, the largest time step size for maintaining the stability is 1/3 instead, and the optimal error reduction rate also changes correspondingly in agreement with the previous analysis.

Figures 4.4 and 4.5 numerically verified the analysis of the optimal error reduction rate in the above section. Note that for the modified scheme, an eigenvalue of the Jacobian matrix is 0, so that along the direction of v, the error disappears in one step. Since $\|v\| = 1$, in the two-dimensional example, v is exactly solved in just one step. This is why even if we set $\mu_2 = 1.5\mu_1$, the optimal error reduction rate is still achieved, which is a special case not covered by the theorem above.

4.2. Other benchmark examples. We now test the algorithm for a number of benchmark problems frequently studied in the literature. First, we consider the Minyaev–Quapp surface [22] given by $E(x, y) = \cos(2x) + \cos(2y) + 0.57\cos(2x - 2y)$.

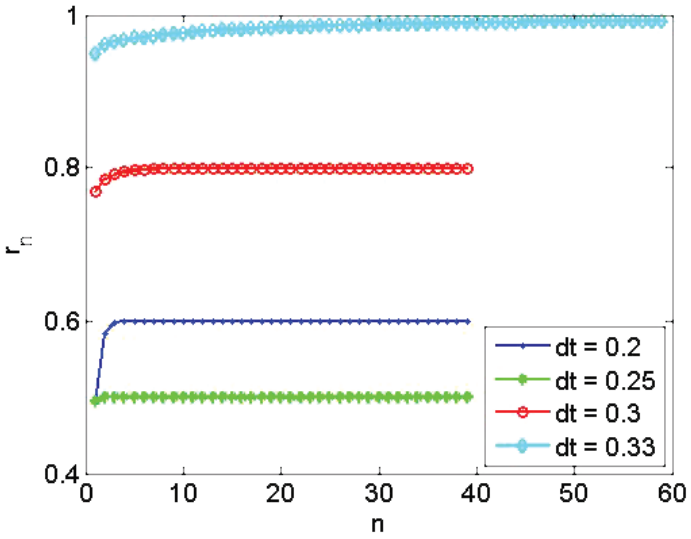

FIG. 4.3. *Error reduction rates for different time step sizes with the modified Euler scheme.*

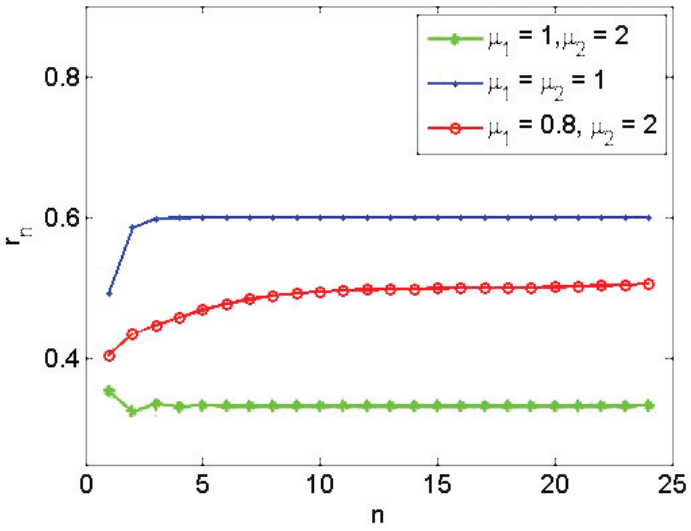

FIG. 4.4. *Error reduction rates for different choices of parameters with the Euler scheme.*

The surface is periodic in space, and in a typical unit cell it has two nearby minima with a saddle point of index-1 situated within the narrow ridge in a relatively flat basin. In Figure 4.6, we show the trajectories of the modified Euler scheme for the starting point $(0.9, 1.2)$ and $(1.5, 0.8)$, respectively. For each case, we take 5 different initial orientation vectors together with $\Delta t = 0.05$ and $\mu_1 = \mu_2 = \mu_3 = 1$ and $l_0 = 0.1$. These initial orientations include one that corresponds to the eigenvector associated with the lowest eigenvalue of the Hessian evaluated at the initial position. The results show the convergence of the trajectories to different saddle points, with the particular

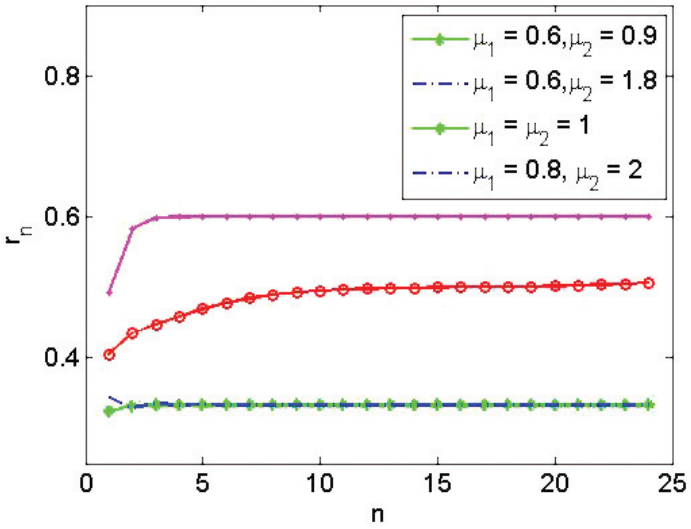

FIG. 4.5. *Error reduction rates for different choices of parameters with the modified Euler scheme.*

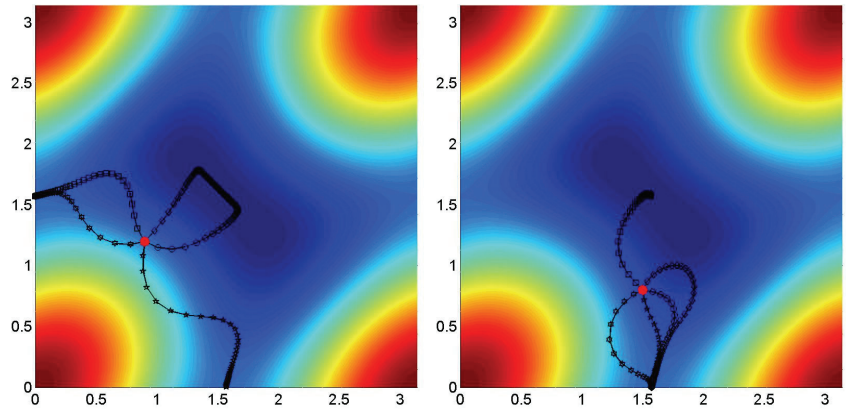

FIG. 4.6. *SDD for Minyaev–Quapp. Left:* $(0.9, 1.2)$. *Right:* $(1.5, 0.8)$.

limiting solution being dependent on the initial orientation vector. For some of the choices, the trajectories can correctly locate the saddle point at the center of the two nearby minima even though the basin of attraction for such a saddle point is very narrow.

Next, we consider the Eckhardt surface [13] given by

$$E(x, y) = \exp(-x^2 - (y+1)^2) + \exp(-x^2 - (y-1)^2) + 4\exp(-3(x^2+y^2)/2) + y^2/2).$$

In Figure 4.7, we show the trajectories of the modified Euler scheme for the starting point $(0.5, 0.7)$ and $(1.2, 1.7)$, respectively. For each case, we again take 5 different initial orientation vectors and use the same set of relaxation constants, initial dimer length, and time step as in the previous example. We see that all trajectories can correctly locate the desired saddle point in these cases.

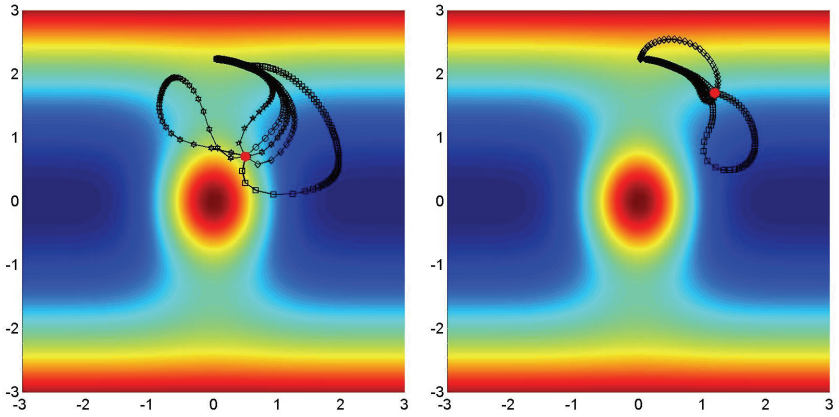

FIG. 4.7. *SDD for Eckhardt surface. Left:* $(0.5, 0.7)$. *Right:* $(1.2, 1.7)$ *(a close-up view).*

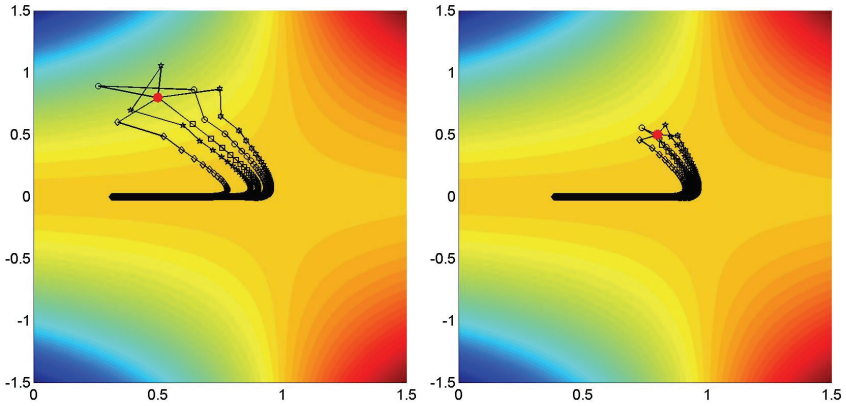

FIG. 4.8. *SDD for stingray function. Left:* $(0.5, 0.8)$. *Right:* $(0.8, 0.5)$.

Finally, we consider the so-called stingray function [15] given by $E(x, y) = x^2 + c(x-1)y^2$, where $c = 100$ is taken. The surface again has a flat ridge which makes it difficult to locate the saddle point. In Figure 4.8, we show the trajectories of the modified Euler scheme for the starting point $(0.5, 0.9)$ and $(0.7, 0.5)$, respectively. For each case, we again take 5 different initial orientation vectors with the same parameters taken as before. All trajectories can correctly locate the desired saddle point in these cases. However, the figure shows that they do not take a direct path to the saddle point; instead, they first climb up to the ridge, then change direction to move along the ridge and finally converge to the saddle.

4.3. An example in infinite-dimensional space: Critical nucleation in phase transformation. As an infinite-dimensional example, the SDD (2.4) is applied to the computation of critical nuclei in phase transformations. Nucleation is a very common physical phenomenon in nature [9, 19, 21, 29, 32]. Our approach is based on the extension of the diffuse interface framework developed originally by Cahn and Hilliard [3]. Further development in [32] allowed the study of critical nuclei morphology in solid state transformations. The simulation results presented here based on the SDD are consistent with those presented in [32] using a different numerical algorithm.

In a diffuse-interface phase-field description where a single order parameter ϕ is used to model the structural difference between the parent phase and the nucleating phase, the free energy at a given temperature is given by a double-well potential

$$f(\phi) = -\phi^2/2 + \phi^4/4 - \rho(3\phi - \phi^3)/4,$$

with two energy wells at $\phi = \pm 1$, and ρ determines the bulk free energy driving force for the phase transformation from the $\phi = -1$ state to the $\phi = 1$ state, i.e., the well depth difference. Let $\Omega = [-1, 1]^2$ be the physical domain on which ϕ is defined; the total free energy over Ω is then given by

$$E(\phi) = \int_\Omega \left[\frac{\gamma_x}{2} \left(\frac{\partial \phi}{\partial x} \right)^2 + \frac{\gamma_y}{2} \left(\frac{\partial \phi}{\partial y} \right)^2 + f(\phi) \right] dx, \tag{4.2}$$

where γ_x and γ_y are constants in Ω to describe the surface energy anisotropy. Setting $\gamma_x = \gamma_y$ leads to the case of isotropic interfacial energy. For simplicity, we omit the misfit elastic energy to simplify the force calculation and leave the more general case to future works. Corresponding to earlier theoretical analysis, the functional (4.2) is defined in an infinite-dimensional function space. By assuming the periodic boundary condition on ϕ, we may take $\mathcal{L} = L^2(\Omega)$ and $\mathcal{H} = H^1_p(\Omega)$, with the latter being the subspace of periodic functions in the conventional Sobolev space $H^1(\Omega)$ to fit the example into the theoretical framework presented earlier.

In the numerical implementation, the infinite-dimensional function spaces are first spatially discretized using Fourier spectral approximations with sufficient number of Fourier modes. When the spatial resolution demands a large number of modes, it is computationally more advantageous to use the semi-implicit scheme discussed earlier. In our nucleation example, the natural force is given by

$$F(\phi) = \gamma_x \phi_{xx} + \gamma_y \phi_{yy} + (1 - \phi^2)(\phi + 3\rho/4)\,. \tag{4.3}$$

We take the semi-implicit Euler scheme of SDD with the linear implicit part given by $F_L(\phi) = \gamma_x \phi_{xx} + \gamma_y \phi_{yy}$, and as in [32]. Figure 4.9 shows the critical nuclei and the corresponding unstable modes, respectively, with $\rho = 0.1$, $\gamma_x = \gamma_y = 4 \times 10^{-4}$ for the isotropic case, and $\gamma_x = \gamma_y/3 = 4 \times 10^{-4}$ for the anisotropic case. The parameters used in the simulation are chosen as $\alpha = 1.5$, $\mu_1 = \mu_2 = \mu_3 = 1$, $l_0 = 10^{-2}$, $\Delta t = 0.8$. We take a sequence of increasing numbers of Fourier modes ranging from $M = 2^8$ to $M = 2^{11}$ to verify that the spatial resolution is adequate, and we terminate the iteration when the L^2 norm of the gradient vector is below 2×10^{-6}. For the isotropic case, the energy and the negative eigenvalue at the computed saddle point all have the same first few significant digits -0.78891 and -0.011326, respectively, for different M, while for the anisotropic case, the energy value and the negative eigenvalue become -0.78079 and -0.011327, thus demonstrating the high spatial resolution of the spectral approximation.

Our numerical experiments also show that for the explicit Euler scheme to work in a numerically stable manner, a much smaller time step Δt has to be taken. For instance, for $M = 2^8$, we need at least $\Delta t < 0.025$, while for $M = 2^{10}$, the step size needs to be smaller than 0.0016. This illustrates the effectiveness of the semi-implicit scheme. Naturally, we may also consider other splitting schemes. These and other improvements to the implementation of the SDD for higher-dimensional problems will be pursued in subsequent works.

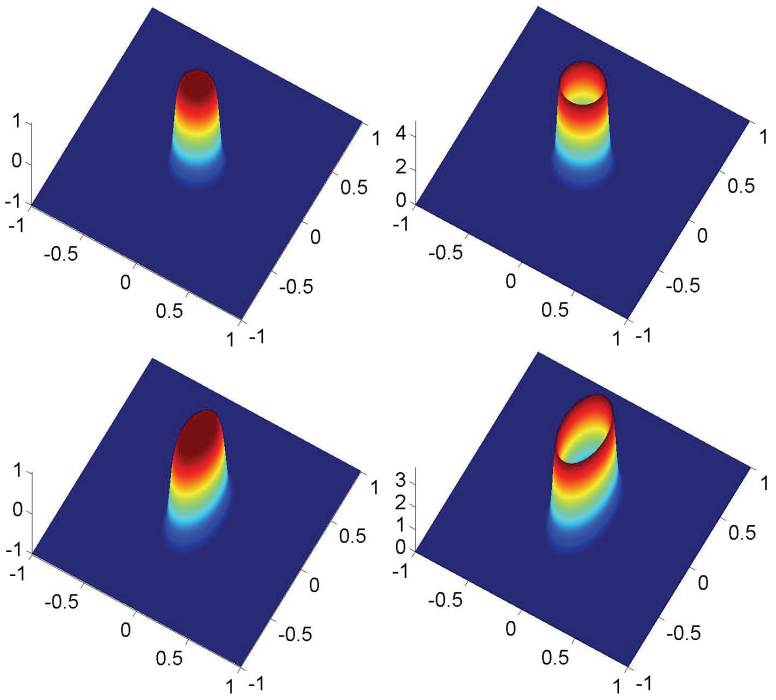

FIG. 4.9. *Critical nuclei and unstable directions with* $\gamma_y/\gamma_x = 1$ *(top row) or* 3 *(bottom row).*

5. Conclusion. We have derived a special shrinking dimer dynamics (SDD) to locate transition states in a given energy landscape, together with theoretical analysis. This dynamic system can avoid the calculation of the second-order derivatives by requiring only the evaluation of the natural forces which corresponds to gradients of the energy. We have presented rigorous analysis for both the continuous dynamic system and its time discretization. We showed in particular the importance of shrinking the dimer length for the guaranteed convergence to saddle points. Our analysis of the time discretization also illustrated that picking suitable relaxation constants for the dimer rotation step may be an equally effective error reduction strategy as doing a full optimization to align the dimer orientation. The latter, which has often been advocated in the literature, obviously carries a much higher computational cost. The SDD has also been successfully applied to solve a number of benchmark problems in lower-dimensional spaces and an infinite-dimensional example of the critical nuclei computation in phase transformations.

While we have focused largely on the index-1 saddle point, it is not difficult to extend the approach to a higher-index case. For example, we may replace a dimer determined by a single orientation vector v by a cluster (a high-dimensional cube, corresponding to setting $\alpha = 1.5$, or a simplex, corresponding to $\alpha = 1$ or 2) spanned by a set of orthonormal vectors. While there is no essential difference in the computational cost for index-1 saddle points with the two different values of α, the high-dimensional cube version involves essentially twice more force evaluations than the simplex version. Such extensions are analogous to the use of Krylov subspaces for eigenvalue problems [31].

On the analysis side, there are still many questions unanswered concerning the global behavior of the SDD as a dynamic system. The linear stability analysis only

provided some local pictures, and global convergence for a more general energy landscape remains to be carried out. The latter is not only technically challenging but also of practical importance. Even though global convergence is not expected for all cases, it is useful to offer some general characterizations of those energy functionals for which global convergence can be assured. On the numerical approximation side, in the discussion of the discretization of the SDD, we considered only the simplest first-order Euler-type schemes. We are currently considering high-order extensions with the objective of maximizing the error reduction per step so as to accelerate the convergence to the equilibrium. Adaptive time steps can also be considered to further enhance the efficiency of discrete algorithms. As the approximate Hessian action along the dimer orientation direction has been utilized in the numerical scheme, one may further combine with quasi-Newton type of iterations to get a superlinear convergence rate, at least along the particular unstable direction of the saddle point. The latter is a feature, for example, of the ART method discussed in [5]. Meanwhile, we may also consider linking the dynamic dimer length to the residuals of the dimer center and dimer orientation equations, or to changes in dimer positions in consecutive iterations, so as to improve the efficiency and robustness of the algorithms. In addition, variations of the SDD that perform constrained saddle point search can also be developed [33].

Furthermore, given the popularity of the dimer methods and other existing saddle point search algorithms, the SDD and its various extensions and discretization can also be used to solve many practical problems such as those related to the study of critical nucleation and chemical reactions. These and other interesting applications will be studied in future works.

Acknowledgments. The authors are grateful to Dr. Lei Zhang and Prof. L.-Q. Chen for providing much assistance on the study of critical nucleation in solid state transformations. They would like to thank Prof. Weinan E for bringing [12] to their attention during the course of this work and for offering his insight on the subject. They also thank the referees for their constructive comments that have helped them improve the manuscript.

REFERENCES

[1] W. Bao and Q. Du, *Computing the ground state solution of Bose–Einstein condensates by a normalized gradient flow*, SIAM J. Sci. Comput., 25 (2004), pp. 1674–1697.
[2] M. Benzi, G. Golub, and J. Liesen, *Numerical solution of saddle point problems*, Acta Numer., 14 (2005), pp. 1–137.
[3] J. Cahn and J. Hilliard, *Free energy of a nonuniform system.* III. *Nucleation in a two-component incompressible fluid*, J. Chem. Phys., 31 (1959), pp. 688–699.
[4] M. Cameron, R. Kohn, and E. Vanden-Eijnden, *The string method as a dynamical system*, J. Nonlinear Sci., 21 (2009), pp. 193–230.
[5] E. Cances, F. Legoll, M.-C. Marinica, K. Minoukadeh, and F. Willaime, *Some improvements of the activation-relaxation technique method for finding transition pathways on potential energy surfaces*, J. Chem. Phys., 130 (2009), 114711.
[6] C. J. Cerjan and W. H. Miller, *On finding transition states*, J. Chem. Phys., 75 (1981), pp. 2800–2806.
[7] G. M. Crippen and H. A. Scheraga, *Minimization of polypeptide energy* XI. *The method of gentlest ascent*, Arch. Biochem. Biophys., 144 (1971), pp. 462–466.
[8] C. M. Dobson, *Protein folding and misfolding*, Nature, 426 (2003), pp. 884–890.
[9] Q. Du and L. Zhang, *A constrained string method and its numerical analysis*, Commun. Math. Sci., 7 (2009), pp. 1039–1051.
[10] W. E, W. Ren, and E. Vanden-Eijnden, *String method for the study of rare events*, Phys. Rev. B, 66 (2002), 052301.

[11] W. E, W. Ren, and E. Vanden-Eijnden, *Simplified and improved string method for computing the minimum energy paths in barrier-crossing events*, J. Chem. Phys., 126 (2007), 164103.
[12] W. E and X. Zhou, *The gentlest ascent dynamics*, Nonlinearity, 24 (2011), pp. 1831–1842.
[13] B. Eckhardt, *Irregular scattering*, Phys. D, 33 (1988), pp. 89–98.
[14] O. V. Galzitskaya and A. V. Finkelstein, *A theoretical search for folding/unfolding nuclei in three-dimensional protein structures*, Proc. Natl. Acad. Sci. USA, 96 (1999), pp. 11299–11304.
[15] W. Grantham, *Gradient transformation trajectory following algorithms for determining stationary min-max saddle points*, in Advances in Dynamic Game Theory, Ann. Internat. Soc. Dynam. Games 9, Birkhäuser Boston, Boston, MA, 2007, pp. 639–657.
[16] G. Henkelman and H. Jonsson, *A dimer method for finding saddle points on high dimensional potential surfaces using only first derivatives*, J. Chem. Phys., 111 (1999), pp. 7010–7022.
[17] G. Henkelman and H. Jonsson, *Improved tangent estimate in the nudged elastic band method for finding minimum energy paths and saddle points*, J. Chem. Phys., 113 (2000), pp. 9978–9985.
[18] G. Henkelman, B. Uberuaga, and H. Jónsson, *A climbing image nudged elastic band method for finding saddle points and minimum energy paths*, J. Chem. Phys., 113 (2000), pp. 9901–9904.
[19] T. Heo, L. Zhang, Q. Du, and L.-Q. Chen, *Incorporating diffuse-interface nuclei in phase-field simulations*, Scripta Mater, 63 (2010), pp. 8–11.
[20] J. Kastner and P. Sherwood, *Superlinearly converging dimer method for transition state search*, J. Chem. Phys., 128 (2008), 014106.
[21] L. Lin, X. Cheng, W. E, A.-C. Shi, and P. Zhang, *A numerical method for the study of nucleation of ordered phases*, J. Comput. Phys., 229 (2009), pp. 1797–1809.
[22] R. M. Minyaev, W. Quapp, G. Subramanian, P. R. Schleyer, and Y. Ho, *Internal conrotation and disrotation in $H_2BCH_2BH_2$ and diborylmethane* 1,3 *H exchange*, J. Comput. Chem., 18 (1997), pp. 1792–1803.
[23] R. Miron and K. Fichthorn, *The step and slide method for finding saddle points on multi-dimensional potential surfaces*, J. Chem. Phys., 115 (2001), pp. 8742–8750.
[24] N. Mousseau and G. T. Barkema, *Traveling through potential energy landscapes of disordered materials: The activation-relaxation technique*, Phys. Rev. E, 57 (1998), pp. 2419–2424.
[25] R. A. Olsen, G. J. Kroes, G. Henkelman, A. Arnaldsson, and H. Jonsson, *Comparison of methods for finding saddle points without knowledge of the final states*, J. Chem. Phys., 121 (2004), pp. 9776–9792.
[26] A. Poddey and P. Blochl, *Dynamical dimer method for the determination of transition states with ab initio molecular dynamics*, J. Chem. Phys., 128 (2008), 044107.
[27] P. Rabinowitz, *Minimax Methods in Critical Point Theory with Applications to Differential Equations*, AMS, Providence, RI, 1986.
[28] C. K. Reddy and H. D. Chiang, *A stability boundary based method for finding saddle points on potential energy surfaces*, J. Comput. Biol., 13 (2006), pp. 745–766.
[29] A. Roy, J. M. Rickman, J. D. Gunton, and K. R. Elder, *Simulation study of nucleation in a phase-field model with nonlocal interactions*, Phys. Rev. E, 57 (1998), pp. 2610–2617.
[30] T. L. Vincent, B. S. Goh, and K. L. Teo, *Trajectory-following algorithms for min-max optimization problems*, J. Optim. Theory Appl., 75 (1992), pp. 501–519.
[31] J. Warsa, T. Wareing, J. Morel, J. McGhee, and R. Lehoucq, *Krylov subspace iterations for deterministic k-eigenvalue calculations*, Nuclear Sci. Engrg., 147 (2004), pp. 26–42.
[32] L. Zhang, L. Q. Chen, and Q. Du, *Morphology of critical nuclei in solid state phase transformations*, Phys. Rev. Lett., 98 (2007), 265703.
[33] J. Zhang and Q. Du, *Constrained shrinking dimer dynamics for saddle point search with constraints*, J. Comput. Phys., 231 (2012), pp. 4745–4758.